

Structural and Optical Studies of Hydrothermal Synthesis of Yttrium Oxide Nanoparticles: *in vitro* Antioxidant Activity

G. MYVIZHI[✉] and S.K. KRISHNA^{*✉}

Department of Chemistry, Chickkaiah Naicker College, Erode-638004, India

*Corresponding author: E-mail: ragul2022@gmail.com

Received: 9 November 2021;

Accepted: 1 December 2021;

Published online: 14 February 2022;

AJC-20698

Nanoparticles research is at the forefront because of its enormous technological potentialities. Through the hydrothermal method, yttrium oxide nanoparticles having multiform morphologies are successfully synthesized. The morphology, structure, photoluminescence properties, and functional groups of these nanoparticles were studied through scanning electron microscopy (SEM), powder X-ray diffraction (PXRD), Fourier-transform infrared spectrometry (FTIR), photoluminescence spectroscopy (PL) and UV-Visible (UV-Vis) analyses. The XRD results showed that the neat samples have cubic Y_2O_3 structure. SEM micrographs revealed that the samples comprised aggregated nanoparticles having different sizes and shapes. The UV-Vis spectra indicated that the absorption peak position shifted towards the lower wavelength with a decrease in the particle size because of the changing surface structures and morphologies. Photoluminescence spectra showed a PL emission with a broad peak at approximately 564 nm, when the sample was excited by 280 nm wavelength. FTIR and EDAX spectra confirmed the presence of metal oxides. Yttrium oxide nanoparticles can counteract the influence of oxidative metabolites and present an antioxidant activity with the IC_{50} of 86.84 $\mu\text{g/mL}$. These properties indicated that these nanoparticles have a potential in biomedical and optoelectronic applications.

Keywords: Nanostructures, Oxides, Hydrothermal synthesis, Luminescence, Yttrium oxide nanoparticles, Biological activity.

INTRODUCTION

In nanomaterials, the particle size is critical for their properties. Physical properties, including luminescence characteristics and band gap of nanomaterials, depend on the size and shape. When the particle size decreases, the volume-to-surface ratio increases and leads to most of the nanomaterial properties. Nanoparticles synthesis is highly challenging for improving the advanced functional materials because nanoparticle show unique properties imparted by the particles with considerably small dimensions and large bulk material [1-3]. Different structures, such as nanoparticles, nanorods, nanospheres, nanotubes, nanocrystals and nanosheets, of rare earth oxide nanostructures present advantageous optical properties, which vary from their bulk counterparts. So, they have received considerable attention. These materials are widely utilized in various fields, including magnetic, optical, thermoelectric fields, and in high power lasers [4,5]. Rare earth oxide nanomaterials provide excellent electrical, optical, and chemical applications compared with

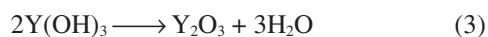
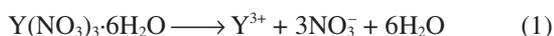
their bulk counterparts. Rare earth oxide materials present various applications for new devices. Yttrium oxide (yttria) is the most promising rare earth oxides and has been studied in recent years. It presents three structural phases, namely hexagonal, cubic and monoclinic [6]. Most of the properties of yttria and the yttria based materials depend on imperfections present inside it and its crystalline form. Yttria is the most potential element utilized in many fields, such as chemical catalysis, optoelectronics devices, high dielectric constant, superconductors, nuclear ceramics and strengthened steels [7]. For luminescent materials that provide a high conversion efficiency, yttria nanoparticles are studied extensively as host matrices due to their large band gaps (5.8 eV), broad optical transparency range and relatively low phonon energies ($\sim 500 \text{ cm}^{-1}$). Moreover, for rare earth ions such as erbium, samarium, europium and gadolinium, it is used as the host material. Yttrium oxide nanoparticles are suitable for luminescence applications because they exhibit corrosion resistivity and high chemical stability [8]. Luminescent rare earth nanoparticles are important in the

development of novel display devices. Yttrium oxide nanostructure preparation has received interest and is encouraged mostly due to its properties such as good thermal conductivity ($33 \text{ W m}^{-1} \text{ K}^{-1}$), high refractory accomplishment (melting point $\sim 2450^\circ\text{C}$), superior chemical stability and excellent mechanical properties. Yttria presents extensive transparency alterations in the violet to infrared range. The toughness and strength of ceramic materials can be enhanced with yttrium oxide addition. It is utilized as an alternative for SiO_2 due to its dielectric characteristic [9-11]. Numerous chemical and physical methods, such as pyrolysis, sol-gel, hydrothermal, combustion and evaporation-condensation synthesis are developed for yttria nanoparticles synthesis. Hydrothermal and sol-gel methods are most widely reported for Y_2O_3 nanoparticles synthesis using KOH and NaOH as precipitating agents [12]. Hence, the present study focuses on the hydrothermal preparation of Y_2O_3 nanoparticles of different morphologies using various precursor concentrations.

EXPERIMENTAL

Synthesis of yttrium oxide nanoparticles: Yttrium oxide nanoparticles were synthesized by hydrothermal method using yttrium nitrate hexahydrate as a precursor and KOH as a precipitating agent. Yttrium nitrate hexahydrate ($\text{Y}(\text{NO}_3)_3 \cdot 6\text{H}_2\text{O}$) with 99.8% purity procured from Merck Specialties Pvt. Ltd. All the chemicals were of analytical grade and used without further purification. An aqueous solution of 0.1 M precursor was taken. An appropriate amount of KOH was added to the precursor to adjust to pH with continuous stirring. The mixture was stirred vigorously for 1 h to achieve homogeneity. Next, the homogeneous mixture was transferred into a 50 mL stainless steel Teflon lined autoclave. The autoclave was heated to 180°C for 6 h. Then, it was air cooled to room temperature. The resulting products were collected through filtration. The products were washed several times with deionized water and anhydrous ethanol and then were dried. Finally, the obtained powders of $\text{Y}(\text{OH})_3$ were placed into ceramic crucible and converted into the corresponding oxide by annealing at 500°C for 3 h in programmable box furnace. The attained final product was used for further characterizations using various concentration of precursor 0.1, 0.2, 0.3 and 0.4 M Y_2O_3 nanoparticles were synthesized and characterized.

Mechanism: The possible chemical reaction for the formation of Y_2O_3 nanoparticles can be expressed as



$\text{Y}(\text{NO}_3)_3 \cdot 6\text{H}_2\text{O}$ decomposes to form Y^{3+} along with its by products as shown in eqn. 1. The OH^- in the base reactant reacts with the acid reactant of Y^{3+} in the solution, resulting in homogeneous precipitation. As per eqn. 2, $\text{Y}(\text{OH})_3$ is formed through the hydrolysis of Y^{3+} followed by the oxidation of O_2 from air to form Y_2O_3 (eqn. 3).

Characterization: The phase and crystal structure of the virgin samples were determined using powder X-ray diffraction

(XRD) using Bruker AXS D8 advance X-ray diffractometer instrument operating at a voltage of 30 kV and a current of 30 mA with $\text{CuK}\alpha$ ($k = 1.5406 \text{ \AA}$) radiation and 2θ angle ranges from 10° to 80° . The surface morphology of the powder samples was characterized by SEM equipped with EDAX EDS detector (Leo, Germany) at an accelerating voltage of 10 kV. The annealed samples of yttrium oxide were dispersed into ethanol and absorption spectrum were recorded by using a Shimadzu spectrophotometer (UV-1700) to measure the band gap in the synthesized sample. The emission spectra were recorded by Cary Eclipse Spectrofluorophotometer under excitation wavelength of 280 nm. The surface functional groups were determined by Perkin-Elmer spectrophotometer in the spectral range of $4000\text{--}400 \text{ cm}^{-1}$.

In vitro antioxidant activity: The antioxidant activity is done by DPPH scavenging assay. In brief, antioxidants scavenge DPPH radicals by donating a proton, thereby forming reduced DPPH. After reduction, the change in colour from purple to yellow can be observed due to a decrease in the absorbance at 517 nm. Various sample concentrations (4 mL) were mixed with 1 mL of a DPPH radicals containing solution, and the final concentration of DPPH of 0.2 mM was achieved. The mixtures were shaken vigorously and allowed to stand constant for 30 min and then the absorbance was determined at 517 nm. Ascorbic acid was utilized as the control. The percentage of inhibition in DPPH radical scavenging activity was calculated as follows [13]:

$$\text{Inhibition (\%)} = \frac{A_0 - A_1}{A_0} \times 100$$

RESULTS AND DISCUSSION

UV-Vis analysis: The room temperature optical absorption spectra were carried out using the instrument of UV-Visible double beam spectrophotometer. Fig. 1 shows the optical absorption of the as-prepared samples of yttria nanoparticles recorded in the wavelength range of 190-1100 nm. The variation in the position of the absorption peak of the as-prepared samples clearly specifies the size dependence of the nanocrystalline materials. The absorbance peak of the as-prepared sample indicates a blue shift, which is essentially owing to the fact that the crystallite size of the as-prepared sample. The sharp absorption peaks occurs at 236, 237, 239 and 242 nm, respectively for 0.1, 0.2, 0.3 and 0.4 M concentration of yttrium oxide samples. Most of the nanomaterials have diverse UV-vis absorption compared with that of the bulk of the same material. The optical band gap energy (E_g) ascribed to the optical absorption limit and can be roughly calculated by the following formula [14]:

$$E_g = \frac{hc}{\lambda}$$

where h is planks constant ($6.626 \times 10^{-34} \text{ Js}$), c is the velocity of light ($3 \times 10^8 \text{ m/s}$) and λ is the optical wave length (378 nm).

The optical band gap energy of yttrium oxide was originated to be 5.25, 5.23, 5.19 and 5.12 eV, respectively for 0.1, 0.2, 0.3 and 0.4 M concentration of Y_2O_3 samples and which

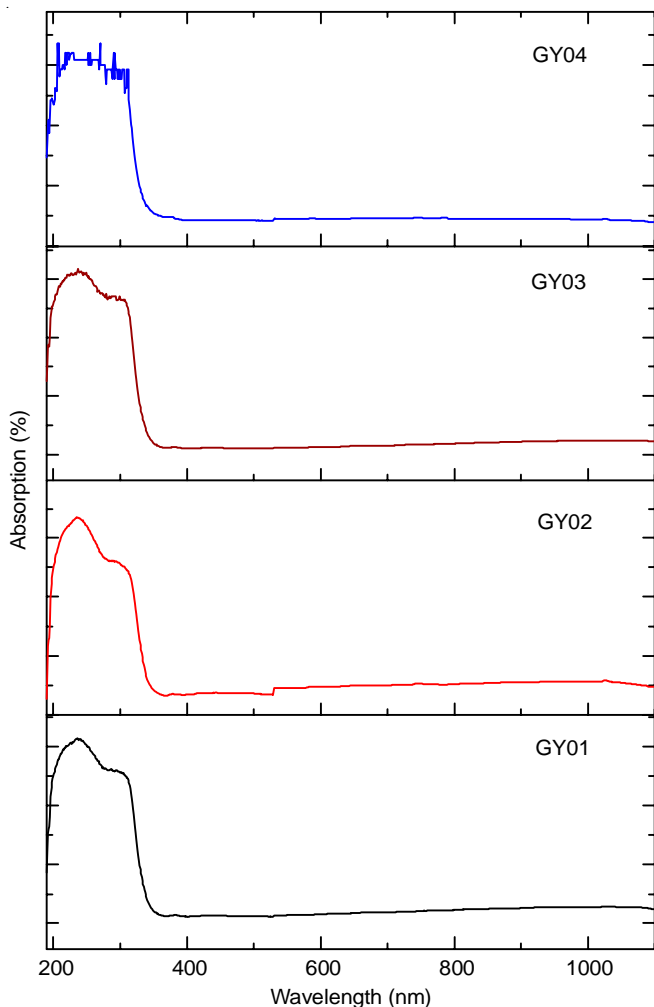


Fig. 1. UV-visible spectra of yttrium oxide nanoparticles

also confirms the blue shift in the UV region [15]. However, these clear and sharp peaks confirmed that the particles are in nanosize and also confirm the narrow particle size distribution.

FTIR analysis: Fig. 2 depicts the FTIR spectra for 0.1, 0.2, 0.3 and 0.4 M of Y_2O_3 nanoparticles made from the instrument of Perkin-Elmer spectrometer in the 4000-400 cm^{-1} region. The spectra of Y_2O_3 nanoparticles displays a broad bands observed at 3538, 3500, 3498 and 3496 cm^{-1} , which are owed to the O-H stretching vibration in H_2O molecules. Subsequently, the weak bands at 1804, 1778, 1778 and 1712 cm^{-1} are ascribed to the O-H deformation vibration. The bands observed at 1579, 1577, 1552 and 1550 cm^{-1} are correspond to different vibrations of carboxylate group, which may originate from CO_2 absorption when exposed to air; some bands have also been observed at 902, 867, 865 and 864 cm^{-1} correspond with the Y-OH stretching mode. The spectra of Y_2O_3 confirm that the intensity of -OH and carbonate groups reduce remarkably. Beside, new absorption bands assigned to the Y-O stretching mode shows at 602, 584, 578 and 574 cm^{-1} signifying the formation of Y_2O_3 nanoparticles from yttrium hydroxide [15,16].

XRD analysis: The powder X-ray diffraction analysis have been carried out using Bruker AXS D8 advance X-ray diffractometer instrument operating at a voltage of 30 kV and

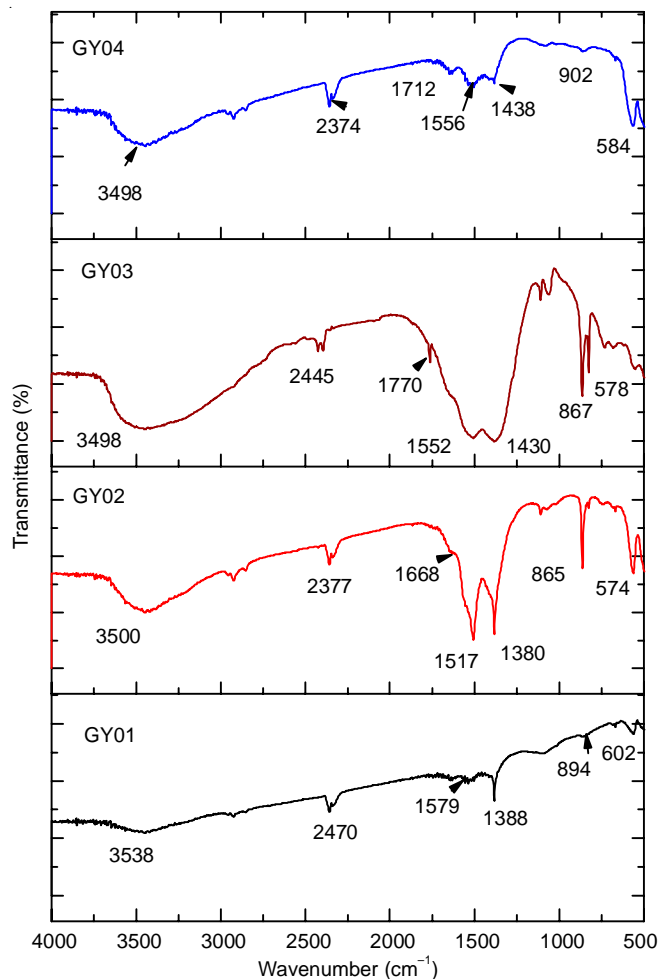


Fig. 2. FTIR spectra of yttrium oxide nanoparticles

a current of 30 mA with $CuK\alpha$ ($k = 1.5406 \text{ \AA}$) radiation and 2θ angle ranges from 10° to 80° . Fig. 3 depicts the PXRD patterns of as prepared Y_2O_3 nanoparticles synthesized using hydrothermal method. It is obviously noticed that these diffraction peaks match completely with the JCPDS card No. 41-1105, given that further validation for the assertion that cubic Y_2O_3 nanoparticles are formed. Further, synthesized Y_2O_3 nanoparticle is also good crystalline in nature, All the perceived diffraction peaks are assigned to various (hkl) planes of cubic crystal system with space group using JCPDS card No: 41-1105 [14]. It is noted that there is improvement of crystallinity with increasing molar concentration. The formation of single phase cubic crystalline yttrium nanoparticles was confirmed. A single phase was formed due to the high *in situ* temperature produced during combustion. The intensity of diffraction peaks increased and the peaks became sharp. The crystallite size 'D' of the samples were evaluated from the XRD line broadening measurement using Scherrer's formula

$$D = \frac{K\lambda}{\beta \cos \theta}$$

where, D is the crystallite size, λ is the wavelength of X-rays (1.5406 \AA), β is the full width at half maxima (FWHM) and θ is the Bragg angle. The average crystallite size is found to be

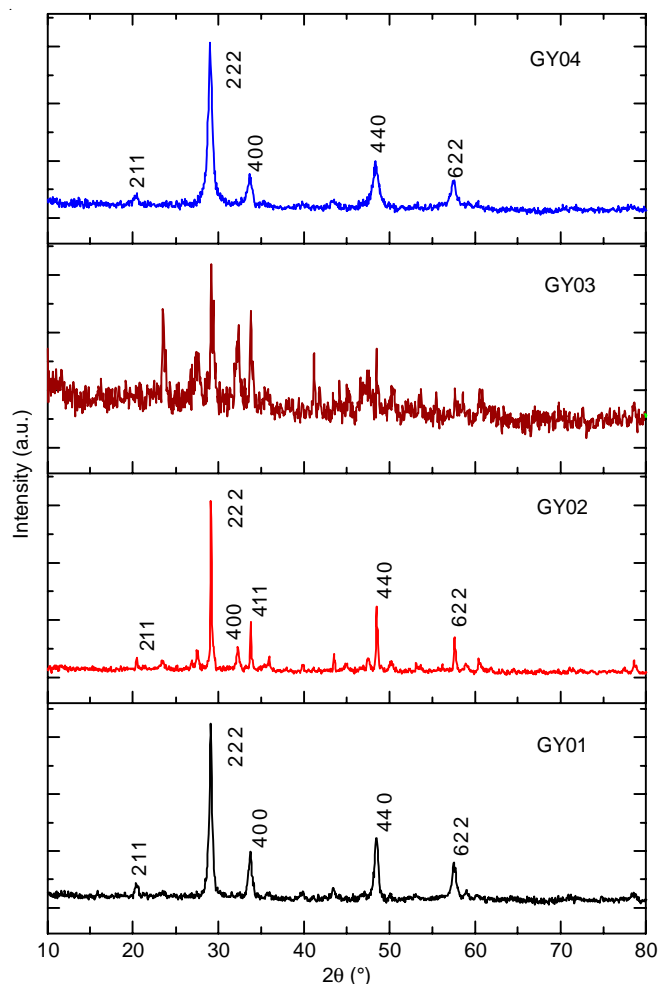


Fig. 3. Powder-XRD pattern of yttrium oxide nanoparticles

in the range 34, 38, 52 and 58 nm for 0.1, 0.2, 0.3 and 0.4 M samples. The crystallite size increases with sample concentration.

The characteristic Bragg diffractions at 2θ values approximately 20.42° , 29.10° , 33.77° , 48.50° and 57.45° are indexed to the (211), (222), (400), (440) and (622) planes, respectively by comparison with JCPDS card No. 41-1105 [17]. The distinct and sharp reflection peaks signify that the product has a high purity and well crystalline particle structure.

SEM analysis: The topography and surface morphology of the synthesized nanoparticles and the microstructure of the synthesized yttrium oxide nanoparticles are shown in Fig. 4a-d. All the four samples of various concentration of Y_2O_3 nanoparticles show the cumulative nature of secondary particles, which are composed of aggregation of numerous primary particles. Contingent upon the precipitating agent employed in the synthesis, the morphology of the sample change. Apparently, the samples of high precursor concentration (0.3 and 0.4 M) exhibits large smooth flat surface along with slight agglomeration of the nanoparticles (Fig.4a-b), whereas the samples of low precursor concentration (0.2 and 0.1 M) are in nanoscale range and have a smooth distribution with rod like structures of different size and shape (Fig.4c-d). The prepared higher molar concentration samples have highly porous structures compare to lower molar concentration samples [18].

EDX analysis: Analysis through energy dispersive X-ray (EDX) spectrometer revealed the occurrence of the characteristic and distinct line of yttrium (Y) and oxygen (O) signal of the Y_2O_3 nanoparticles and no impurities were occurrence in the synthesized materials which is depicted in Fig. 5a-d. The weight and atomic percentage data of element were also revealed using EDX spectrum and presented in Table-1.

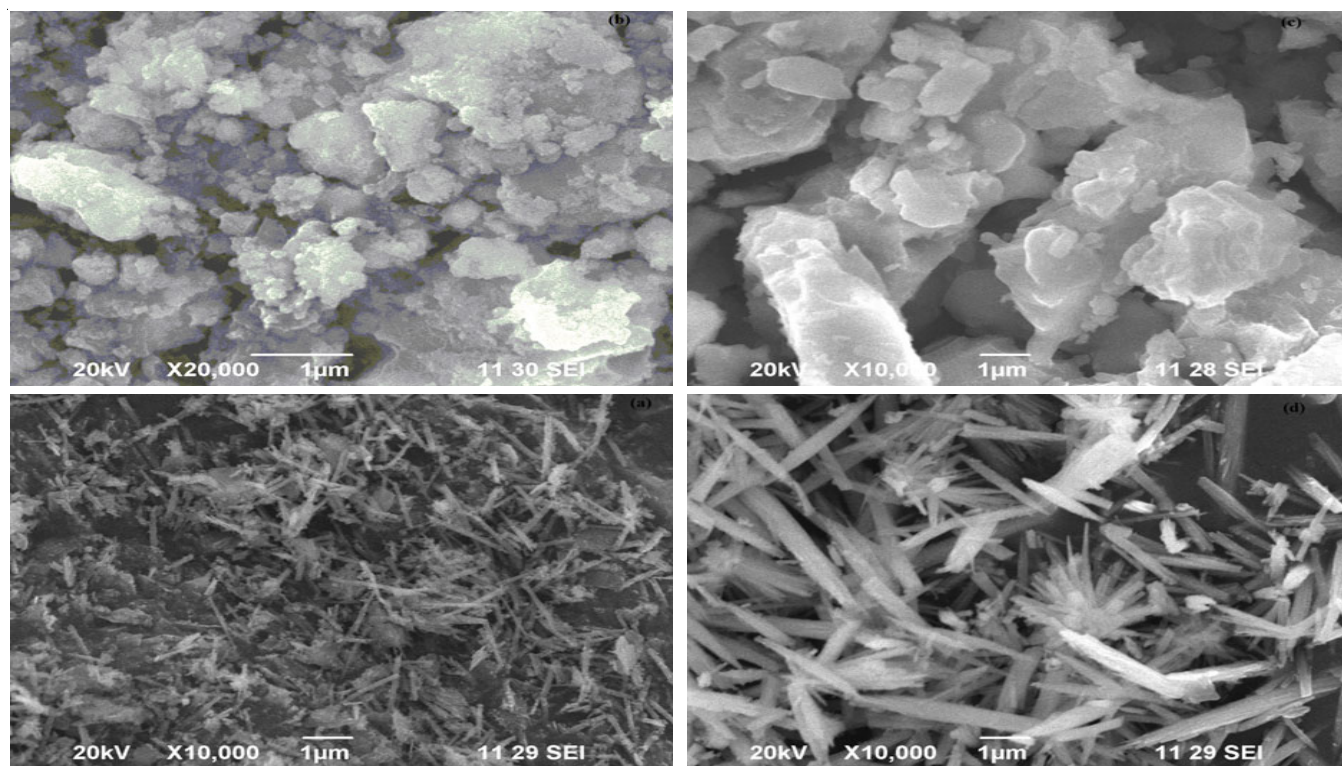


Fig. 4. SEM images of yttrium oxide nanoparticles

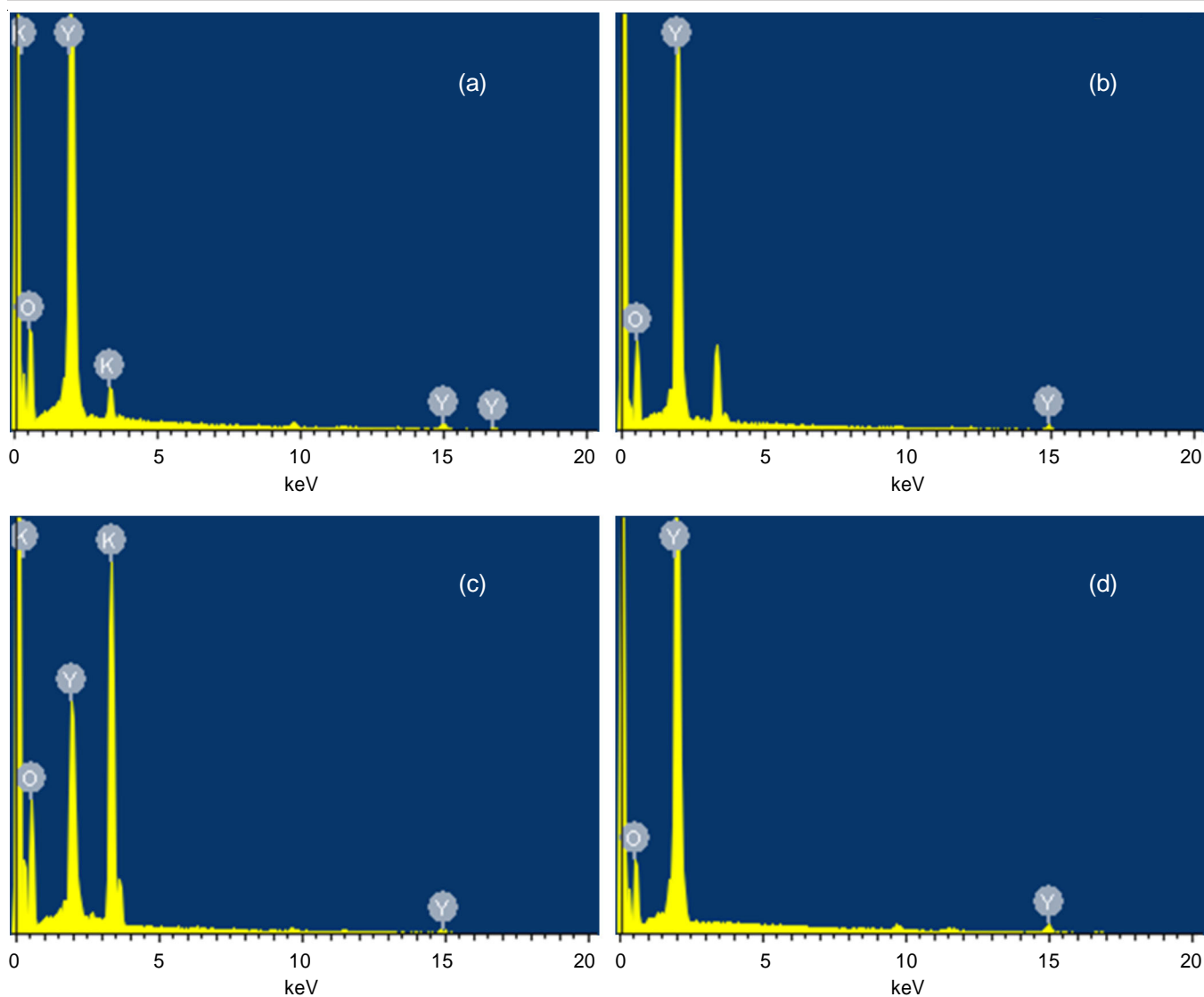


Fig. 5. EDX spectra of yttrium oxide nanoparticles

Sample name	O	K	Y
0.1 M	38.10	2.90	58.99
0.2 M	41.38	–	58.62
0.3 M	48.73	27.76	23.51
0.4 M	33.30	–	66.70

Optical studies: The photoluminescence (PL) spectra of the as-prepared 0.1, 0.2, 0.3 and 0.4 M Y_2O_3 nanoparticles are shown in Fig. 6. All the samples exhibit three emission peaks at about 360, 382 and 564 nm. The peaks at 360 nm might be due to the presence of oxygen vacancies related to radiative recombination. At 564 nm, Y_2O_3 nanoparticles showed a strong orange emission peak. The broad excitation band for yttrium oxide was caused by the charge transfer of O_2^- to Y^{3+} [19]. Osipov *et al.* [20] reported cathodoluminescence with peaks at 515–640 nm and emission was due to the recombination of $Y_3^+-O_2^-$ (donor-acceptor) pair. These reported luminescence peaks match with this study. In this study, photoluminescence arise

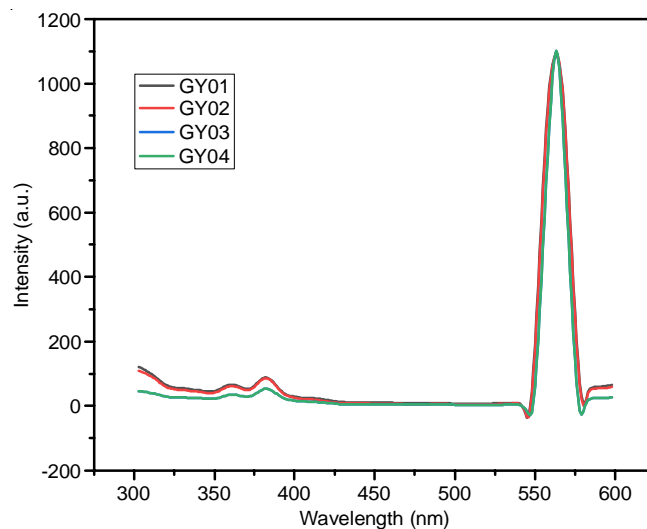


Fig. 6. PL emission spectrum of yttrium oxide nanoparticles

emission peaks obtained at 386 nm are attributed to the oxygen vacancy defects including F-centres and those at 564 nm might

TABLE-2
PERCENTAGE OF INHIBITION IN DIVERSE CONCENTRATIONS (20,40,60 AND 100 µg/mL) OF YTTRIUM OXIDE NANOPARTICLES

	Inhibition (%)				
	20 µg/mL	40 µg/mL	60 µg/mL	80 µg/mL	100 µg/mL
Sample	10.73 ± 0.25	21.60 ± 0.50	33.44 ± 0.20	46.20 ± 0.30	56.55 ± 0.50
Standard (ascorbic acid)	13.68 ± 0.40	25.50 ± 0.70	37.59 ± 0.23	49.12 ± 0.30	61.20 ± 0.10

due to the crystallite size increase. The growth of crystallite size leads to a decrease in nonradiative transition and -OH and C=O impurity vibration, which causes the increase in PL emission intensities [21]. However, the PL intensity is higher in this study than in previous work possibly due to crystallinity enhancement [22].

in vitro antioxidant activity: The antioxidant activity of fabricated Y₂O₃ nanoparticles was estimated as free radical scavenging activity. In DPPH method, the free radical reacts with antioxidants and its colour changes from purple to light yellow after reduction. DPPH exhibits an unpaired electron on the nitrogen atom and the π-system. On aromatic ring, exchange increases molar absorptive. This effect is important when substituents lead to an increase in the conjugation length. Extended conjugation causes shifts in benzene absorption bands from a shorter to longer wavelength. The peak at 517 nm corresponds to the n→π* energy transition [23]. The RSA of the synthesized Y₂O₃ nanoparticles increased with the increase in the Y₂O₃ nanoparticle concentration. The results showed significant RSA in synthesized Y₂O₃ nanoparticles from 10.73% to 56.55% with an IC₅₀ value of 86.84 µg mL⁻¹, while positive control ascorbic acid offered 61.20% inhibition at 100 µg mL⁻¹ and the values are shown in Table-2. Further, the obtained result indicates that the Y₂O₃ nanoparticles have high antioxidant property.

Conclusion

Nanocrystalline yttrium oxide was synthesized effectively using the hydrothermal method. The cubic phase of Y₂O₃ nanoparticles was confirmed through XRD. The crystallite size was 34-58 nm. The effect of the particle size on optical properties was proven on the basis of UV-vis and photoluminescence results. The photoluminescence (PL) emission with a high PL intensity and broad peaks near 360, 384, and 564 nm was observed in the synthesized samples because of crystallinity enhancement. The SEM images of Y₂O₃ nanoparticles revealed the rod-like structure of loosely agglomerated particles. These particles were crispy, fluffy with voids and pores and having the energy gap of 5.19-5.25 eV. The synthesized Y₂O₃ nanoparticles exhibited significant antioxidant potential which is on par with the standard drugs. The Y₂O₃ nanoparticles sample synthesized at 0.1 M concentration possess nanorods like morphology, good crystallinity and superior role in multifunctional modalities and hence can be epitomized as potential luminescent material for optoelectronic and biomedical applications.

CONFLICT OF INTEREST

The authors declare that there is no conflict of interests regarding the publication of this article.

REFERENCES

- K. Ariga, J.P. Hill, M.V. Lee, A. Vinu, R. Charvet and S. Acharya, *Sci. Technol. Adv. Mater.*, **9**, 014109 (2008); <https://doi.org/10.1088/1468-6996/9/1/014109>
- G.S. Yi and G.M. Chow, *J. Mater. Chem.*, **15**, 4460 (2005); <https://doi.org/10.1039/b508240d>
- I. Denry and J.A. Holloway, *Materials*, **3**, 351 (2010); <https://doi.org/10.3390/ma3010351>
- X. Gao, L. Yang, J.A. Petros, F.F. Marshall, J.W. Simons and S. Nie, *Curr. Opin. Biotechnol.*, **16**, 63 (2004); <https://doi.org/10.1016/j.copbio.11.003>
- B.C. Jamalajah, J.S. Kumar, A.M. Babu and L.R. Moorthy, *J. Alloys Compd.*, **478**, 63 (2009); <https://doi.org/10.1016/j.jallcom.2008.12.013>
- Y.C. Cao, *J. Am. Chem. Soc.*, **126**, 7456 (2004); <https://doi.org/10.1021/ja0481676>
- P.C. Ray, H. Yu and P.P. Fu, *J. Environ. Sci. Health C Environ. Carcinog. Ecotoxicol. Rev.*, **27**, 1 (2009); <https://doi.org/10.1080/10590500802708267>
- V. Bondar, *Mater. Sci. Eng. B Solid-State Mater. Adv. Technol.*, **69-70**, 505 (2000); [https://doi.org/10.1016/S0921-5107\(99\)00310-4](https://doi.org/10.1016/S0921-5107(99)00310-4)
- O.A. Graeve, S. Varma, G. Rojas-George, D.R. Brown and E.A. Lopez, *J. Am. Ceram. Soc.*, **89**, 926 (2006); <https://doi.org/10.1111/j.1551-2916.2006.00845.x>
- A. Towata, M. Sivakumar, K. Yasui, T. Tuziuti, T. Kozuka and Y. Iida, *J. Mater. Sci.*, **43**, 1214 (2008); <https://doi.org/10.1007/s10853-007-2287-1>
- T. Mokkelbost, I. Kaus, T. Grande and M.A. Einarsrud, *Chem. Mater.*, **16**, 5489 (2004); <https://doi.org/10.1021/cm048583p>
- R. Srinivasan, R. Yogamalar and A.C. Bose, *Mater. Res. Bull.*, **45**, 1165 (2010); <https://doi.org/10.1016/j.materresbull.2010.05.020>
- K. Shimada, K. Fujikawa, K. Yahara and T. Nakamura, *J. Agric. Food Chem.*, **40**, 945 (1992); <https://doi.org/10.1021/jf00018a005>
- R. Srinivasan, N.R. Yogamalar, J. Elanchezhian, R.J. Joseyphus and A.C. Bose, *J. Alloys Compd.*, **496**, 472 (2010); <https://doi.org/10.1016/j.jallcom.2010.02.083>
- X. Liu, F. Zhou, M. Gu, S. Huang, B. Liu and C. Ni, *Opt. Mater.*, **31**, 126 (2008); <https://doi.org/10.1016/j.optmat.2008.02.001>
- C.A. da Silva, N.F.P. Ribeiro and M.M.V.M. Souza, *Ceram. Int.*, **35**, 3441 (2009); <https://doi.org/10.1016/j.ceramint.2009.06.005>
- A. J. Abdulghani and W. M. Al-Ogedy, *Iraqi J. Sci.*, **56**, 1572 (2015).
- A. Konrad, U. Herr, R. Tidecks, F. Kummer and K. Samwer, *J. Appl. Phys.*, **90**, 3516 (2001); <https://doi.org/10.1063/1.1388022>
- J. Bang, M. Abboudi, B. Abrams and P.H. Holloway, *J. Lumin.*, **106**, 177 (2004); <https://doi.org/10.1016/j.jlumin.2003.09.005>
- V.V. Osipov, A.V. Rasuleva and V.I. Solomonov, *Opt. Spektrosk.*, **105**, 524 (2008); <https://doi.org/10.1134/S0030400X08100068>
- A.E. Souza, G.T.A. Santos, B.C. Barra, W.D. Macedo Jr., S.R. Teixeira, C.M. Santos, A.M.O.R. Senos, L. Amaral and E. Longo, *Cryst. Growth Des.*, **12**, 5671 (2012); <https://doi.org/10.1021/cg301168k>
- B. Karmakar, T. Som, S.P. Singh and M. Nath, *Trans. Indian Ceram. Soc.*, **69**, 171 (2010); <https://doi.org/10.1080/0371750X.2010.11090834>
- R. Dobrucka, *J. Inorg. Organomet. Polym. Mater.*, **28**, 812 (2018); <https://doi.org/10.1007/s10904-017-0750-2>